Human Molecular Genetics, 2009, Vol. 18, No. 11 ***1924–1936***
doi:10.1093/hmg/ddp114
Advance Access published on March 17, 2009

Molecular mechanisms for subtelomeric rearrangements associated with the 9q34.3 microdeletion syndrome

Svetlana A. Yatsenko[1], Ellen K. Brundage[1], Erin K. Roney[1], Sau Wai Cheung[1], A. Craig Chinault[1] and James R. Lupski[1,2,3,*]

[1]Department of Molecular and Human Genetics, [2]Department of Pediatrics, Baylor College of Medicine and [3]Texas Children's Hospital, Houston, TX 77030, USA

Received January 12, 2009; Revised February 16, 2009; Accepted March 9, 2009

We characterized at the molecular level the genomic rearrangements in 28 unrelated patients with 9q34.3 subtelomeric deletions. Four distinct categories were delineated: terminal deletions, interstitial deletions, derivative chromosomes and complex rearrangements; each results in haploinsufficiency of the *EHMT1* gene and a characteristic phenotype. Interestingly, 25% of our patients had *de novo* interstitial deletions, 25% were found with derivative chromosomes and complex rearrangements and only 50% were bona fide terminal deletions. In contrast to genomic disorders that are often associated with recurrent rearrangements, breakpoints involving the 9q34.3 subtelomere region are highly variable. Molecular studies identified three regions of breakpoint grouping. Interspersed repetitive elements such as *Alu*, LINE, long-terminal repeats and simple tandem repeats are frequently observed at the breakpoints. Such repetitive elements may play an important role by providing substrates with a specific DNA secondary structure that stabilizes broken chromosomes or assist in either DNA double-strand break repair or repair of single double-strand DNA ends generated by collapsed forks. Sequence analyses of the breakpoint junctions suggest that subtelomeric deletions can be stabilized by both homologous and nonhomologous recombination mechanisms, through a telomere-capture event, by *de novo* telomere synthesis, or multistep breakage-fusion-bridge cycles.

INTRODUCTION

Submicroscopic deletion of the distal long arm of chromosome 9, del(9)(q34.3), is a relatively newly described genomic rearrangement disorder that affects fetal development and results in mental retardation and multiple congenital anomalies. Constitutional deletions of the distal long arm of chromosome 9 [del(9)(q34.3), OMIM 610253] encompassing the *EHMT1* (euchromatic histone methyltransferase 1) gene, or loss-of-function mutations in *EHMT1*, result in a clinically recognizable syndrome that is characterized by specific craniofacial features, hypotonia, childhood obesity, microcephaly and substantial speech delay and mental retardation (CHOMS) (1–4). The number of patients identified has been increasing significantly with widespread application of high-resolution genome analysis technologies such as array comparative genomic hybridization (array-CGH) (5). Microdeletions of 9q34.3, like other terminal deletions, have breakpoints occurring in multiple sites but are limited to the ~4 Mb subtelomeric region. The virtual lack of detection of larger terminal deletions by conventional cytogenetics at the 9q34 chromosome region in live births is thought to reflect lethality (i.e. haplolethal effects) in early embryogenesis.

Most human subtelomeric regions consist of gene-rich, light-staining GTG-bands that are difficult to visualize cytogenetically by G-banding chromosome analysis. The end of every human chromosome consists of 3–20 kb of tandemly repeated $(TTAGGG)_n$ telomere sequences (6), which are essential for chromosome stability. Telomeres function as a protective 'cap' at the chromosome terminus to prevent fusion and degradation and to help distinguish intact chromosome ends from damaged chromosomes (7,8). Immediately adjacent to the terminal $(T_2AG_3)_n$ simple sequence repeats are 100–300 kb of 'telomere-associated repeats' (TAR).

*To whom correspondence should be addressed at: Department of Molecular and Human Genetics, Baylor College of Medicine, One Baylor Plaza, Room 604B, Houston, TX 77030, USA. Tel: +1 7137986530; Fax: +1 7137985073; Email: jlupski@bcm.tmc.edu

TAR sequences have homologies shared between multiple chromosome ends (9,10). Unique, chromosome-specific DNA is located proximal to the TAR sequence. Molecular studies employing a series of probes for FISH or array-CGH analyses showed that many subtelomere deletions are more complex than anticipated. Understanding the molecular mechanism resulting in 9q34.3 subtelomeric microdeletion will provide insight into the mechanisms of genomic rearrangements and particularly terminal chromosome rearrangements.

RESULTS

Clinical features of patients with 9q34.3 microdeletion syndrome

Patients with deletions of distal 9q34 included 15 females and 13 males, with ages ranging from 10 months to 42 years (Table 1). There was considerable clinical variability among the patients, although all patients except P41 showed a characteristic phenotype compatible with the 9q34.3 microdeletion syndrome. These manifestations include a distinctive craniofacial appearance, relative microcephaly, feeding difficulties, hypotonia and significant delay or absence of expressive speech. We have proposed the acronym CHOMS (craniofacial features, hypotonia, obesity, microcephaly and speech delay) to succinctly summarize the predominant clinical features (3). Interestingly, patient P41 is a 16-year-old girl who was referred for genetic testing due to mental retardation and behavioral problems, and her clinical picture did not fit with CHOMS. She was born to a healthy mother with no family history of mental retardation, congenital anomalies or metabolic disorders, but who is positive for a 9q34.3 deletion detected by subtelomere FISH studies.

Molecular characterization of 9q34 deletions

A total of 29 individuals (28 patients and the mother of P41) were analyzed by array-CGH using a high-resolution custom 9q34 oligonucleotide microarray to determine the genomic size, extent and gene content of the deletions. The deletion size in three patients (P3, P4 and P22) had been determined previously using BAC/PAC and fosmid clones for FISH or array-CGH studies (3,5), and breakpoints are further refined in this study. The deletion size, extent and genomic content were determined to 0.5–6 kb resolution. In patients with terminal deletions, deletion size is approximated as calculated from the breakpoint to the end of the chromosome 9 assembly (UCSC hg18). Four distinct categories of rearrangements were observed: terminal deletions ($n = 14$), interstitial deletions, complex rearrangements of 9q34 and derivative chromosome 9 (resulting in double-segmental imbalance) (Fig. 1, Table 1).

The deletions in 14 subjects were terminal (Fig. 1A), 6 patients (P21, P26, P28, P34, P42, P44) had interstitial deletions (Fig. 1B), 2 patients (P6 and P29) had complex deletion/duplication rearrangements with multiple breakpoints within 9q34 (Fig. 1C), and a derivative chromosome 9 was present in 5 cases (P11, P16, P19, P22, P38) (Fig. 1D). The deletions differed in size from 0.164 to 3.129 Mb, and in 27 patients (all except P41) the 9q deletion encompassed either the entire or a portion of the *EHMT1* gene. In P41, as well as in her healthy mother, the 9q34.3 deletion breakpoint was located in intron 6 of the *CACNA1B* gene, ~83.8 kb downstream of *EHMT1* (Fig. 1A). Therefore, deletion encompassing the *CACNA1B* gene in this family most likely represents a copy number variant (CNV) not associated with mental retardation or behavioral problems. Thus, on the basis of our analysis, we were able to exclude a diagnosis of 9q34.3 microdeletion syndrome which was previously established in this family.

Twenty-five rearrangements (90%) were *de novo*, one patient (P16) presented with a derivative chromosome segregating from a balanced parental translocation, one patient inherited the deletion from her mother (P41), and samples from parents of P38 were not available for study. Breakpoints on the partner chromosomes were established by FISH or array-CGH studies for P11, P19 and P38. In patients P16 and P19, breakpoints on the partner chromosomes were located within the satellite of the short arm of chromosome 13 and a repetitive pericentromeric sequence of 15q11.2, respectively; therefore, their junction sequences cannot be determined precisely. In addition, several recurrent intervals of gains or losses were identified within the distal 10 Mb segment of chromosome 9 that may represent CNVs (Supplementary Material, Table S1).

Parental origin of the deletion

Parental origins of 9q34.3 rearrangements were examined in 19 families. Interestingly, in 11 patients, *de novo* 9q deletions occur on a paternal chromosome (65%), whereas in six subjects, deletions were of maternal origin (35%) (Fig. 2B). Two patients, P16 and P41, inherited a derivative 9 and a small 9q deletion from their mothers, respectively. A complex rearrangement in P6 was found to occur on the maternal chromosome.

Breakpoint junction analyses

High-resolution array-CGH delineated the proximal and distal flanking regions of the deletion and allowed the design of oligonucleotide primers to amplify the junction fragments. Using this strategy, seven deletion junction fragments were isolated including three from cases with interstitial deletions (P26, P37, P44; Fig. 3), two with terminal deletions (P3, P40; Fig. 4), one case with a derivative chromosome 9 (P38; Fig. 5) and one patient with a complex rearrangement (P29; Fig. 6A). The inability to capture other breakpoints may relate to the complexity of the genomic sequence at the breakpoint, our inability to uniquely identify the genomic location of the breakpoint due to its occurrence within repetitive sequences or the complexity of the mechanism generating the breakpoints, which would be incompatible with our tacit underlying assumptions in the experimental design to amplify the junction sequences.

An array-CGH result and primer design are shown for P44 with an interstitial deletion (Fig. 3). This patient was found to have a deletion encompassing 658 kb, and two breakpoints were expected within an ~500 bp proximal and 805 bp distal breakpoint regions (Fig. 3A). Forward primers 'A',

Table 1. Delineation of rearrangements in 28 patients with 9q34.3 deletions

Patient	Gender	Karyotype	Rearrangement	9q34.3 deletion size[a], Mb	Associated genome imbalance, size
P3	F	del(9)(q34.3)dn	Terminal deletion	1.143	None
P4	F	del(9)(q34.3)dn	Terminal deletion	0.753	None
P6	M	der(9)del(9)(q34.3)dup(9)(q34.3q34.2)tri(9)(q34.2q34.2)dn	Complex	0.834	dup(9q34.3q34.2), tri(9)(q34.2q34.2), 3.4 Mb
P7	M	del(9)(q34.3)dn	Terminal deletion	1.539	None
P8	M	del(9)(q34.3)dn	Terminal deletion	0.914	None
P10	M	del(9)(q34.3)dn	Terminal deletion	0.753	None
P11	F	der(9)t(9;9)(p24;q34.3)dn	Derivative chromosome	0.353	dup(9p24pter), 8 Mb
P12	M	del(9)(q34.3)dn	Terminal deletion	2.983	None
P13	M	del(9)(q34.3)dn	Terminal deletion	2.139	None
P14	F	del(9)(q34.3)dn	Terminal deletion	3.249	None
P16	M	der(9)t(9;13)(q34.3;p11.2)mat	Derivative chromosome	2.120	dup(13p12-pter)
P19	F	−15,der(9)t(9;15)(q34.3;q11.2)dn	Derivative chromosome	2.245	del(15)(q11.2pter), 1.7 Mb
P21	F	del(9)(q34.3q34.3)dn	Interstitial deletion	0.707	None
P22	M	der(9)t(2;9)(q13;q34.3)dn	Derivative chromosome	2.720	Not determined
P26	M	del(9)(q34.3q34.3)dn	Interstitial deletion	0.651	None
P28	F	del(9)(q34.3q34.3)dn	Interstitial deletion	0.546	None
P29	M	der(9)(q34.3q34.3)dn	Complex	0.945	None
P34	F	del(9)(q34.3q34.3)dn	Interstitial deletion	0.233	None
P35	M	del(9)(q34.3)dn	Terminal deletion	0.542	None
P36	F	del(9)(q34.3)dn	Terminal deletion	0.753	None
P37	F	del(9)(q34.3q34.3)dn	Interstitial deletion	0.164	None
P38	F	der(9)t(5;9)(q35.3;q34.3)	Derivative chromosome	0.567	dup(5)(q35qter), 96 kb
P39	M	del(9)(q34.3)dn	Terminal deletion	1.669	None
P40	F	del(9)(q34.3)dn	Terminal deletion	2.942	None
P41	F	del(9)(q34.3)mat	Terminal deletion	0.339	None
P42	M	del(9)(q34.3q34.3)	Interstitial deletion	0.176	None
P43	F	del(9)(q34.3)dn	Terminal deletion	0.995	None
P44	F	del(9)(q34.3q34.3)dn	Interstitial deletion	0.658	None

[a]The total size is calculated between breakpoints or between breakpoint and the end of the chromosome 9 assembly (UCSC hg18).

'B' and 'C' were designed at ∼120 and 200 bp intervals from each other and used with the reverse primer 'D', and, therefore, the expected products AD, BD and CD should be of different sizes. We were able to amplify across the deletion, producing three PCR products that were ∼670, 850 and 970 bp in size, consistent with sizes predicted from primer positions (Fig. 3B). As expected, these junction fragments were amplified from the patient genomic DNA, but not from the parental or control DNAs. The smallest ∼670 bp fragment was sequenced, and the 678 bp junction fragment showed 303 bp unique to the proximal region and 375 bp unique to the distal region. There was no homology identified between the breakpoint-flanking regions, but two repetitive sequences, a 72 bp low-complexity repeat and 312 bp *AluSq*, were present 50 nucleotides (nt) proximal and 52 nt distal from the proximal and distal breakpoints, respectively. The deletion junction fragments in P26 and P37 were obtained and analyzed using the same approach as described earlier (data not shown). Sequence analyses in P26 or P37 showed no large homology segments between the proximal and distal sequences flanking the breakpoints. The junction fragment in P26 had a microhomology of three bases and an insertion of a single T-base (Fig. 3C). These data suggest that the interstitial deletions were most likely formed by a nonhomologous-end-joining (NHEJ) recombination mechanism.

For all 14 patients with apparent terminal deletions of the 9q34.3 region that were identified in this study, array-CGH revealed losses encompassing the most distal unique sequence of 9qter (Fig. 4A). However, it is possible that some of these deletions might not be 'true' terminal deletions, but interstitial with a distal breakpoint located within the TAR sequences. We attempted to clone deletion breakpoints in cases where the truncated 9q was healed apparently by the addition of a new telomere repeat sequence at the distal site. Two patients P3 and P40 were identified with *de novo* telomere synthesis at the broken end, and results of our investigation for P40 are shown in Fig. 4. Two forward primers 'K' and 'L' were designed within the 1500 bp breakpoint region on 9q and used for PCR together with a reverse primer 'TEL' complementary to the telomere repeat (Fig. 4A). Two junction fragments LTEL and KTEL were amplified and sequenced using the forward primer 'L' (Fig. 4B and C). Sequence analyses of the junction fragments in P3 and P40 (Fig. 4D) revealed a 5 bp 'AGGGT' and a 2 bp 'GG' microhomology at the fusion point of unique and telomere sequences. Interestingly, these microhomology sequences are included within the canonical TTAGGGTTAGGG telomere repeat and may reflect the template-driven replication mechanism that the ribonucleotide protein telomerase utilizes to replicate chromosome ends.

Five patients in our series have a derivative chromosome 9 with a deletion due to unbalanced translocation or a telomere-capture event. In these cases, the proximal region was determined precisely in all patients, but distal sequences on the 'donor' chromosome were determined only in P11 and P38. The high-resolution 9q34 microarray analysis on P38 identified loss of a 447 kb segment on distal 9q34.3 and a gain encompassing the most distal region of chromosome 5q (Fig. 5A). FISH studies with 9q and 5q subtelomere-specific

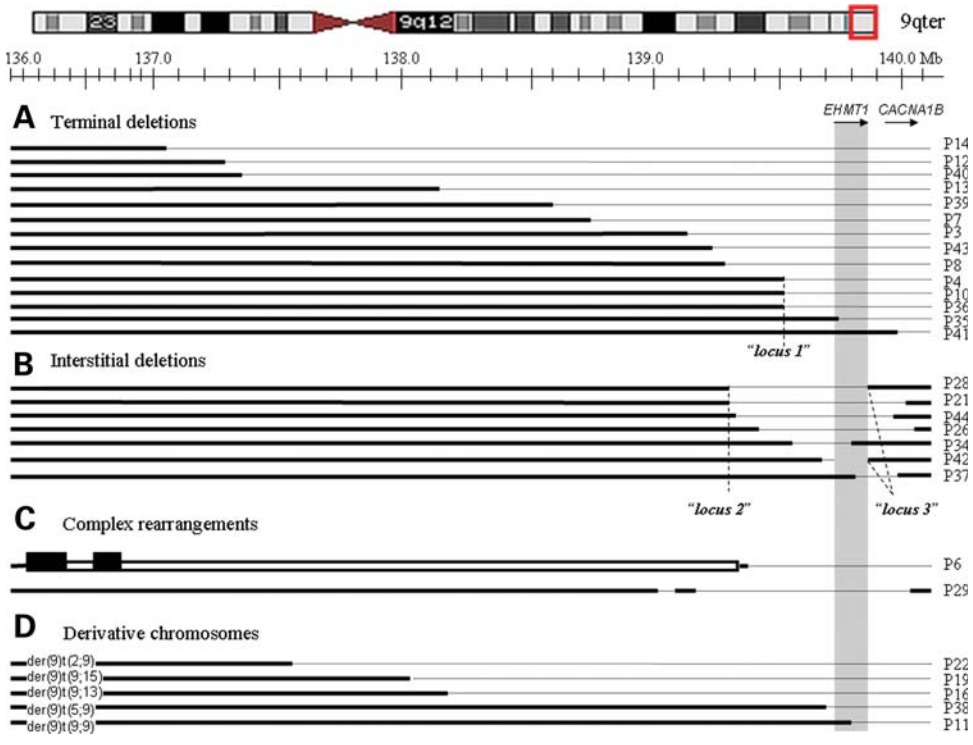

Figure 1. Schematic representation of the 9q34.3 rearrangements in 28 patients identified by array-CGH. An ideogram of chromosome 9 is shown at the top with genomic coordinates of the boxed terminal region of interest shown below at 100 kb intervals. The locations of the *EHMT1* and *CACNA1B* genes are marked by horizontal arrows demarcating the direction of transcription. The genomic region of the *EHMT1* gene is shown as a gray box. Non-deleted chromosome regions are represented by thick black horizontal lines. The deleted region in each patient is indicated by a thin dashed line. The double black line in P6 corresponds to the duplicated region, and black rectangles indicate triplicated intervals. Three loci of deletion breakpoints grouping are indicated.

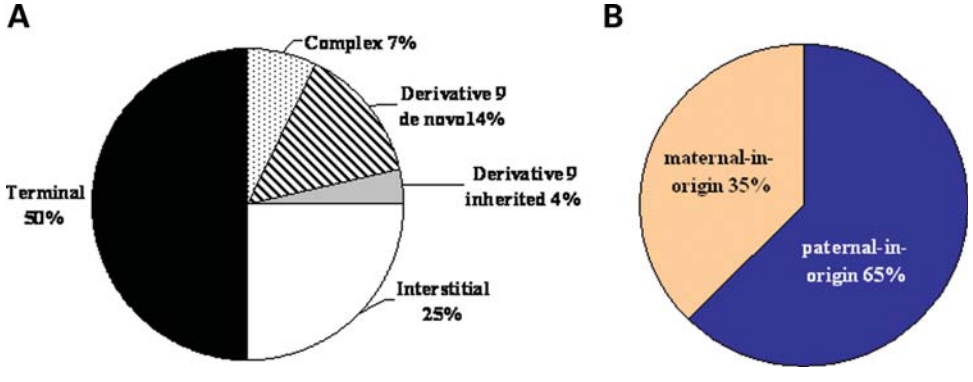

Figure 2. (**A**) A pie chart depicting distribution of different types of rearrangements associated with the 9q34.3 microdeletion syndrome. (**B**) Distribution of cases according to the parental origin of the 9q34 rearrangements.

probes revealed an additional copy of 5qter located on the deleted chromosome 9q (Fig. 5B). To amplify the junction region between 9q34.3 and 5q35.3 sequences, we performed PCR using forward primer 'H' from the 9q34.3 deletion-flanking region and a reverse primer 'J' corresponding to the 5q duplicated segment. Sequencing of the junction fragments in both directions revealed a breakpoint within a 295 bp *AluSg* element on chromosome 9q that shares 83% homology between *AluSg* sequences on 5q. These data suggest that the broken chromosome 9 was stabilized by capture of an existing telomere via interchromosomal recombination between homologous *Alu* elements by a nonallelic homologous recombination (NAHR) event.

The majority of constitutional chromosomal aberrations are thought to be simple rearrangements. The incidence of complex chromosome rearrangements (CCRs) was considered to be very low; however, the frequency of such events can be significantly underestimated and depends on the resolution of the method used for genome analysis. Using high-resolution array-CGH, we identified two patients P6 and P29 with CCRs involving the 9q34.3 region. In P29, four breakpoints were identified resulting in two interstitial deletions of 61 kb

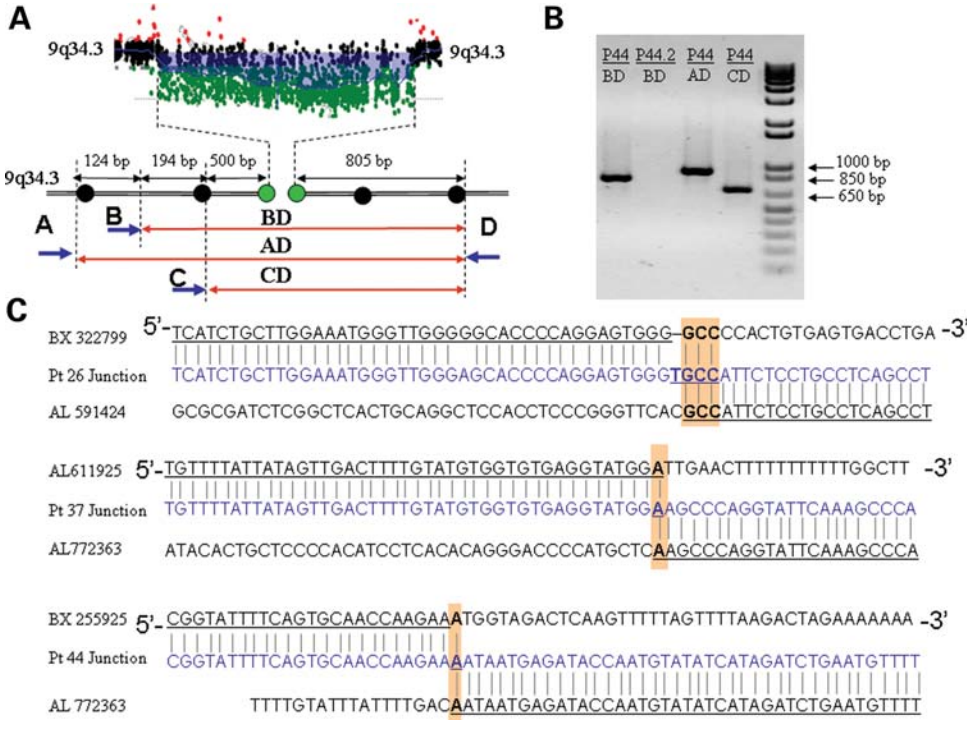

Figure 3. Molecular cloning of interstitial 9q34.3 deletions. (**A**) A magnified view of the breakpoint boundary detected by array-CGH using an oligonucleotide-based custom 9q34 microarray. The shaded area indicates a loss in DNA copy number (deletion) detected by oligonucleotide probes (green dots). Black dots represent probes with no change in copy numbers (non-deleted region). Below is a schematic view of the breakpoint junction. Double black lines indicate 9q34.3 unique subtelomere DNA sequence. Blue arrows show locations of PCR primers for the cloning of the breakpoint junction. (**B**) Amplification of junction fragments in P44. Three products AD, BD and CD are shown. Deletion in P44 was found to be paternal in origin, so amplification with primers 'B' and 'D' was also carried out using the father's genomic DNA (P44.2), which was negative for a junction fragment. (**C**) DNA sequences spanning the deletion junctions in P26, P37 and P44 with interstitial 9q34.3 deletions aligned with the reference sequences. The microhomology regions across the deletion junction are highlighted by yellow boxes. Dashes indicate gaps introduced to maximize the alignments.

and 940 kb in size (Fig. 6A). A relatively small 65 kb region encompassing four genes interrupted the deleted segment. A duplication involving this region was previously found among normal individuals and could represent a CNV. To rule out the possibility of a contiguous interstitial deletion on one chromosome 9 and duplication on the homologous 9, we performed a FISH analysis using fosmid clones within the region of interest.

Also, to exclude an inversion involving the 65 kb nondeleted segment, we used a different combination of primers localized within sequences flanking each of the four breakpoints. We were able to amplify a junction fragment using proximal and distal oligonucleotides flanking the 61 kb deletion which was not seen in either parent or the control, consistent with this rearrangement representing a *de novo* CCR. Sequence analysis of the junction fragment identified a microhomology consistent with a potential NHEJ recombination (Fig. 6B). However, the absence of an information scar [i.e. addition or loss of nucleotide(s) at the junction] and the observed 3 bp microhomology could also be consistent with a Fork Stalling Template Switching (FoSTeS) model (11).

CCR including deletion, duplication and interspersed microtriplication of 9q34 was identified in P6 (Fig. 6C). Conventional cytogenetic analysis showed additional chromosome material at the distal long arm of the chromosome (Fig. 6D). Further BAC/PAC array-CGH performed elsewhere determined a 1 Mb deletion of 9q34.3 and an inverted duplication of the more proximal 9q34.3–q34.2 region. Surprisingly, our study revealed a more complex rearrangement with at least six breakpoints. We identified a terminal deletion that was separated with a duplication region by a 9 kb unaltered sequence. In addition, two triplicated segments were scattered more proximally (Fig. 6C). FISH analyses showed that these triplicated sequences are located at the terminal end of the derivative 9q (data not shown). Both parents had normal chromosome and FISH analyses, indicating *de novo* complex rearrangements in a child. The interrupted deletion/inverted duplication structure is consistent with a breakage–fusion–bridge (BFB) cycle mechanism, which was first described by McClintock (8). However, the presence of an interrupted triplication at the end of aberrant 9q suggests either a multistep healing event or a FoSTeS mechanism.

Breakpoint DNA-sequence analyses in patients with 9q34. 3 deletions

Forty-three breakpoints within the 9q34 region were identified and characterized at 0.5–6 kb resolution. Interestingly, 30 breakpoints (~70%) occurred within the most distal 1.2 Mb region of chromosome 9, whereas there were only 4–5 breakpoints in each of the more proximal 1 Mb genomic segments. Our analyses revealed that the majority of the 9q34.3

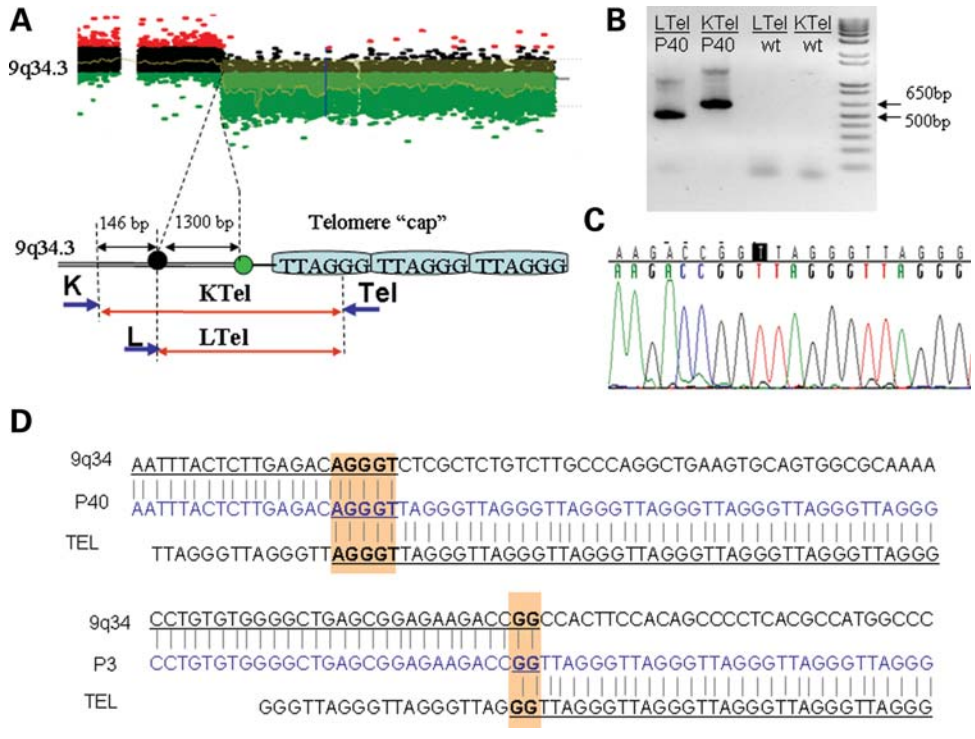

Figure 4. Molecular cloning of the terminal 9q34.3 deletions. (**A**) An array-CGH profile in P40 showing a 9q34.3 terminal deletion. Below is a schematic view of the breakpoint junction. The blue portion designated as 'telomere cap' indicates a telomere $(TTAGGG)_n$ sequence. Blue arrows show locations of PCR primers 'K', 'L' and 'TEL' for cloning the breakpoint junctions. (**B**) Two junction fragments were obtained in P40. Neither junction was observed using the same PCR primers (LTEL/wt, KTEL/wt) in the PCR to amplify the genomic DNA of the parent from which the rearranged chromosome originated, demonstrating that both junctions are *de novo* in P40. (**C**) Direct sequencing of the amplified fragment in P3 revealed the breakpoint junction between the 9q34.3 proximal region and the telomere specific $(TTAGGG)_n$ repeat sequence. (**D**) DNA sequence spanning the deletion junctions in P3 and P40 with terminal deletions. The proximal region is aligned to the 9q reference sequence and telomere $(TTAGGG)_n$ repeat sequence present at the distal region of the junction sequence. The homologous nucleotides at the breakpoints are shown in yellow shaded boxes.

breakpoints were unique and scattered along the most distal 3.2 Mb interval. However, three loci of breakpoint grouping were detected. Three patients (P4, P10 and P36; Fig. 1) had terminal deletions with a breakpoint located within a 2.8 kb sequence ('locus 1', chr9: 139 516 706–139 519 570; hg 18) of intron 13 of the *PNPLA7* gene. Two proximal breakpoints in patients with interstitial deletions (P21 and P28) were found within an ~6 kb interval ('locus 2', chr9: 139 301 499–139 307 607; hg18). Two distal breakpoints in patients with interstitial deletions (P28 and P42) occurred in a 2.7 kb region ('locus 3', chr9: 139 854 004–139 856 674; hg 18). These regions may represent 'hotspots' with sequence motifs that either facilitate or stabilize deletion formation. Analysis of the breakpoint sequences revealed a significantly high incidence ($\chi^2 = 8.71$; $P < 0.003$) of repetitive elements such as simple tandem repeats (STRs); short-interspersed nuclear elements (SINEs), including *Alu* sequences; long-interspersed nuclear elements (LINEs), such as L1M and L2; and long-terminal repeats (LTRs), which include retroposons (Table 2). Twenty-three breakpoints out of 30 (76%) observed within the most telomeric 1.2 Mb region were associated with repetitive elements, whereas the repetitive elements account for ~42% of the sequence.

We hypothesized that differences of breakpoints distribution along the 9q34.3 region may correlate with the density of various interspersed repetitive elements. We calculated interspersed repetitive element densities within the unique sequence of the 9q most distal 3 Mb region. Content of repetitive sequences of the most distal 135 kb segment, the 9q TAR region, has been calculated separately. Approximately, 38% of the subtelomere 9q region consists of repetitive elements including LINEs, SINEs and LTRs (Fig. 7A). Remarkably, the number of the breakpoints observed at a given location seems to correlate specifically with LINE repeat sequence content (Fig. 7A,B), especially within the interval up to 2 Mb from the 9q TAR. However, such a correlation was not observed within the genomic region 2–3 Mb from the TAR sequence. It has been noted that 9q34.3 deletions over 3 Mb in size are rare. Thus, breakpoints within this genomic interval spanning 2–3 Mb from the 9q terminus may occur relatively frequent; however, these may be associated with a more severe phenotype or lethality.

We performed secondary structure prediction analysis of ssDNA from the three loci in which selected breakpoints were apparently grouped using the Mfold Web software. Remarkably, 'locus 1' and 'locus 3' sequences are predicted to fold into stem-loop or loop configurations, which is similar to a telomere $(TTAGGG)_n$-repetitive sequence t-loop structure (Fig. 8A–C). In contrast, the folding of a 6 kb 'locus 2' sequence (Fig. 8D) and a 2.6 kb sequence at the breakpoint in P3 (Fig. 8E) and P40 (Fig. 8F) revealed a complex secondary structure characterized by extensive

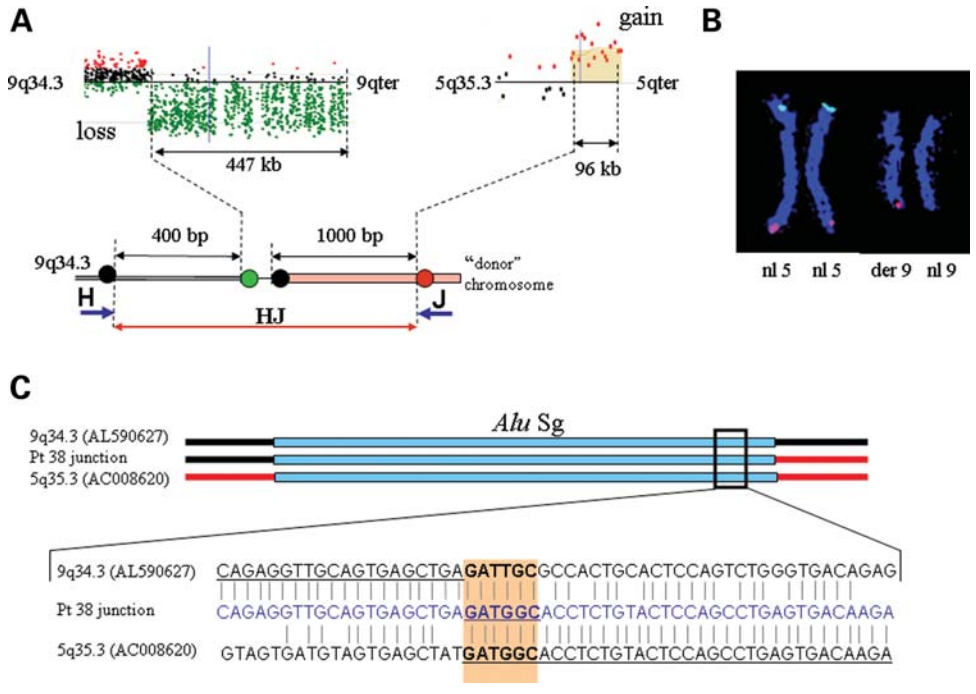

Figure 5. Molecular cloning of the 9q34.3 deletions in P38 with a derivative chromosome. **(A)** Chromosome 9q and 5q array-CGH profiles showing a loss of 9q34.3 and a gain in DNA copy number within the subtelomere 5q region. Below is the schematic representation of the aberrant chromosome 9. (**B**) FISH analysis using the 5q (red signal) and 5p (green signal) subtelomere-specific probe revealed an extra signal on the distal 9q. (**C**) Sequence alignment of 60 bp around the junction. The sequence of the deleted chromosome (in the middle) is shown with the proximal and distal reference sequences of normal chromosome 9 (top and bottom). Nucleotides present at the junction are in bold and highlighted by the yellow shaded box; dashes indicate gaps to maximize the alignments.

DNA bending with hairpins and loops, and potentially unstable structures. Our breakpoint analyses showed that in P3 and P40, the broken 9q was stabilized by a telomere-repetitive sequence.

DISCUSSION

Several common syndromes, such as monosomy 1p36 (OMIM 607872), Wolf-Hirschhorn (OMIM 194490), Cri-du Chat (OMIM 123450), monosomy 9p (OMIM 158170), 9q34.3 microdeletions (OMIM 610253), Jacobsen (OMIM 147791), Miller–Dieker (OMIM 247200) and 22q13.3 (OMIM 606232) are associated with terminal subtelomeric deletions of chromosomes 1p, 4p, 5p, 9p, 9q, 11q, 17p and 22q, respectively. With the widespread application of high-resolution genomic analyses, a substantial number of rearrangements involving the subtelomeric regions of all chromosomes have been reported to cause birth defects and mental retardation (12–14). Many of these deletions are not mediated by low-copy repeats (LCRs), are of different size and genomic content in each patient, commonly cannot be resolved by conventional cytogenetic techniques and thus might be classified as nonrecurrent rearrangements associated with genomic disorders (15). Although a characteristic phenotype has been recognized for a few of these rearrangements, little is known about the contribution to the phenotype potentially made by either dosage-sensitive genes or regulatory elements within the deleted region. Furthermore, there is a paucity of information available regarding either molecular recombination mechanisms leading to terminal deletions or genome architectural features potentially causing susceptibility to genomic instability.

Submicroscopic deletion del(9)(q34.3) is a relatively newly described genomic disorder that affects fetal development and results in mental retardation and multiple congenital anomalies. Microdeletions of the 9q34.3 region, like other terminal deletions, have breakpoints occurring in multiple sites of the distal chromosome end. Molecular analysis of patients with monosomy 1p36 (16) or 9p21–p24 (16,17) demonstrated that deletions vary widely up to 20 Mb in size with no single common breakpoint. In patients with monosomy 1p36, 40% of all breakpoints were located 3.0–5.0 Mb away from the telomere (16), so >50% of these rearrangements can be detected by chromosome analysis. In contrast to monosomy 1p36, and 9p syndromes, deletions involving the 9q34.3 region do not exceed 3.5–4 Mb in size; therefore, such rearrangements are usually beyond the resolution of conventional cytogenetic techniques.

In our study, ~70% of 9q34.3 breakpoints occurred within the most distal 1.2 Mb region (Fig. 1). Our studies demonstrate that rearrangements of the 9q34.3 region can be either paternal or maternal in origin. Paternally derived rearrangements were usually *de novo* simple terminal deletions (65% of patients), whereas interstitial deletions, complex rearrangements and unbalanced translocations were frequently maternal in origin. Moreover, the majority of small 9q34.3 deletions (<1.2 Mb) were paternal, whereas deletions >1.2 Mb in size were predominantly maternal in origin. In contrast, 60% of patients with monosomy 1p36 had small deletions on the maternally derived chromosome, whereas paternal deletions were larger. Interest-

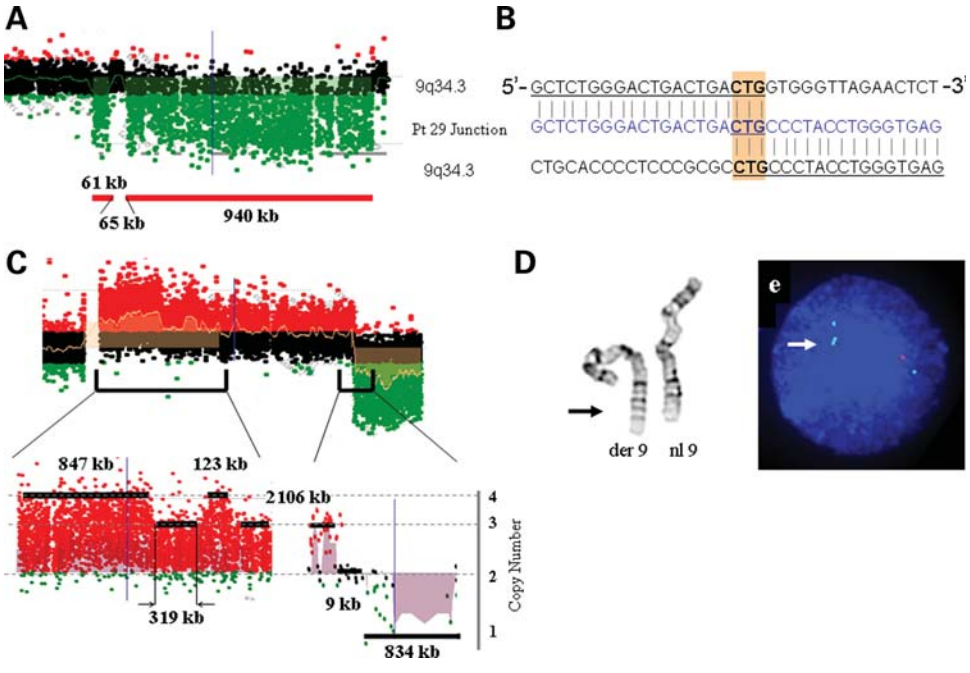

Figure 6. Molecular cloning of the 9q34.3 deletions in patients with complex rearrangements. **(A)** Array-CGH profiles in P29 showing a complex interrupted deletion within the 9q34.3. Red line indicates the deleted segments. (**B**) DNA sequences spanning the 61 kb deletion junction in P29 aligned with the reference sequences. The microhomology regions across the deletion junction are highlighted by yellow boxes. (**C**) Array-CGH profiles in P6 showing a complex-interrupted deletion/duplication/triplication rearrangement. Below is the magnified view of the breakpoint regions. Black thick lines indicate a DNA copy number within the 9q34.2–q34.3 region. The most 9q34.3 telomeric region is deleted; proximally adjacent region showing no copy number alteration; duplicated (three copies)/triplicated (four copies) segments were scattered more proximally. (D) Interphase FISH analysis using clones RP11-188C12 (AL611925; red) and RP11-54A22 (AL591890; green) showing a deletion of the distal 9q34.3 and triplication of the 9q34.2 region in P6.

ingly, the distal 9q34.3 region has significant differences in recombination rates between maternal and paternal chromosomes (18,19). Within the segment located 3 Mb away from the 9q telomere, female- and male-specific recombination rates were calculated as 3.5 and 3.7 cM/Mb, respectively, whereas in the most distal 1 Mb region, recombination events in females were not detected at all, and in males, the recombination rate was found to be 1.8 cM/Mb. For the 1p36 region, the peaks of recombination are observed within segments located 4–5 and 5–6 Mb away from the telomere in females and males, respectively (18). It is possible that location and parental origin of DNA breaks correlates with the recombination map. Thus, nonrecurrent breakpoints observed in patients with subtelomere rearrangements may not be entirely random, but rather more common within specific regions or sequences of the human genome.

The ends of chromosomes are evolutionarily active with a very high rate of meiotic recombination and double-strand breaks (DSBs). Elevated recombination rates within the subtelomeric regions may depend on GC content, density or content of genes, *cis*- and *trans*-genetic modifiers, chromatin structure or may be associated with specific genomic sequence features. Specific genomic architectural features such as LCRs and short-interspersed repetitive elements (e.g. *Alu*) are known to mediate recurrent rearrangements including deletions, duplications, inversions and translocations via NAHR (20). Such sequences may stimulate, but do not mediate, rearrangements due to NHEJ and FoSTeS (21). NHEJ has been implicated in pathogenesis of subtelomeric nonrecurrent rearrangements as well (22,23). From our junction analysis, we conclude that interstitial deletions in three patients were consistent with NHEJ repair.

The presence of short repetitive elements has been proposed to play a role in generating or stabilizing the terminal deletions; however, it is unclear whether these repeats participate in a recombination events or are involved in DNA replication and repair. In this study, we have determined 43 breakpoint junctions within the subtelomeric 9q34.3 region. Repetitive sequences such as *Alu*, LINE, SINE, LTRs and STRs were commonly present at or near the breakpoints (Table 2). These repetitive elements are susceptible to DSBs due to replication errors or by formation of unusual DNA secondary structures including cruciforms, hairpins, triplexes, tetraplexes and so on. (24). In addition, secondary structure can inhibit DNA polymerization or accumulate ssDNA in the replication fork, thus increasing the probability of rearrangements.

A DNA replication model termed FoSTeS has been proposed to explain the complex rearrangements associated with Pelizaeus–Merzbacher disease (OMIM 312080) (11). This long-distance template-switching replication mechanism has been postulated for *Escherichia coli* gene amplification (25) and for both disease-associated rearrangements and CNVs in the human genome (26,27). The microhomology mediated break-induced replication (MMBIR) model represents a more generalized mechanism with specific molecular details and applicable to all life forms. In the FoSTeS/MMBIR model, a DNA replication fork stalls or pauses at DNA lesions, leading to fork collapse and the generation of a single ended double strand DNA, and subsequent restoration of replication

Table 2. Genomic features at the 9q34 breakpoint region in each patient

Patient	Genomic features at the breakpoint region
P3	None
P4, P10, P36	AluJb, AluSq, AluSx, L1MC5, STRs
P6	—
P7	STRs
P8	AluJo, AluSg, AluY, LTR (MER68, ERVL-C1), L1M, STRs
P11	—
P12	AluY, L2
P13	L2, STRs
P14	STRs
P16	—
P19	—
P21	AluJo
P22	Tandem segmental duplications
P26	AluY
P28	AluY, L1M5
	AluSp, AluY, L1MC4a, L1ME1, STRs
P29	AluSx
P34	STRs
P35	Simple repeat $(TGG)_n$
P37	AluSc, L1ME4a
P38	*Alu Sg*
P39	None
P40	LTR
P41	None
P42	AluSx, AluSq, AluJb, L1M5
P43	None
P44	None

by switching to an alternative template using microhomology to prime DNA synthesis on the switched template. Among patients reported in this study, two subjects were found with complex 9q34 rearrangements. Rearrangement in P6 is suggestive of a multistep healing event. Interestingly, a patient with a complex rearrangement including deletion, inverted duplication and triplication of the distal 9q34.3 region has been reported recently (28). These findings provide additional evidence that diverse mechanisms may be involved in generating subtelomeric chromosomal rearrangements. The deletion segment in P29 was interrupted by a small nondeleted segment. Similarly, multiple deletions were reported previously in three patients with monosomy 1p36 syndrome (16). Analysis of a junction fragment in P29 revealed a 3 bp microhomology. Rearrangements resulting in complex multiple deletions may be explained by coincidence of independent DSBs events healed by NHEJ mechanism, although the frequency of such aberrations is likely to be extremely low. Alternatively, interrupted deletions and more complex rearrangements can be more parsimoniously explained by the FoSTeS/MMBIR mechanism.

In this study, 50% of patients were detected with simple terminal deletions. In the absence of functional telomeres, eukaryotic chromosomes undergo end-fusion and degradation events, making them generally unstable. At least three mechanisms for healing of terminal deletions have been proposed: *de novo* telomere addition mediated by telomerase, capture of an existing telomere resulting in derivative chromosomes and stabilization by BFB cycles, consistent with interrupted terminal deletion and more proximal inverted interrupted duplication rearrangement. Each of these mechanisms has been identified by characterization of terminal deletions (28–32) and also is revealed in the present study.

In the reported cases, the truncated chromosomes have been healed by the direct addition of T_2AG_3 repeats onto nontelomeric sequences. Despite high-resolution array-CGH analysis for the majority of patients with terminal deletions, attempted amplification of the junction fragments was nonproductive. Molecular studies employing a series of probes for FISH or array-CGH analyses showed that many terminal deletions are more complex than anticipated. In our PCR design, we hypothesized healing by the T_2AG_3 repeats, but not TAR sequences for telomere swaps; the latter may not be spanned by a long PCR designed to amplify the junction. However, some of the terminal abnormalities may be interstitial rearrangements with a distal breakpoint within TAR repeats or be complex as well.

In contrast to recurrent rearrangements that are often associated with genomic architectural features, breakpoints involving the subtelomeric region are highly variable. Molecular studies identified three regions of breakpoint grouping within the 9q34.3 region. Interestingly, unique breakpoints have been reported for most subjects with nonrecurrent deletions involving the 22q13.3 region, but a recurrent breakpoint within a small region of the *SHANK3* gene has been identified in three individuals (33). The loci of breakpoint grouping may represent hot spots with a specific DNA sequence feature or a secondary structure that stabilizes broken chromosome or assist in DNA DSB repair or loading of the telomerase enzyme.

This study shows that multiple mechanisms associated with subtelomeric DNA alterations and repair can be involved in the pathogenesis of the 9q34.3 microdeletion syndrome. The observed mechanisms can also be implicated in rearrangements of other subtelomeric regions; some of these models may be more prevalent depending on chromosome region-specific characteristics, such as genomic architecture, repetitive sequence density or other genomic features. More investigations are required to further understand the mechanisms and frequencies with which they are involved in subtelomeric rearrangements.

MATERIALS AND METHODS

Human subjects

This study was approved by the Baylor College of Medicine (BCM) Institutional Review Board and affiliated hospitals. We identified 28 unrelated patients with deletions of distal chromosome 9q34.3 region (Table 1). Blood samples were obtained from patients and their parents after informed consent. Twenty-three patients had normal high-resolution G-banded chromosome analysis and were ascertained through either abnormal subtelomere FISH or array-CGH studies at BCM or elsewhere. Five patients had an abnormal karyotype, with structural rearrangements involving the distal long arm of chromosome 9.

Array-CGH studies

A custom high-resolution 9q34 array was designed using a 44K array format (Agilent Technologies, Inc., Santa Clara, CA,

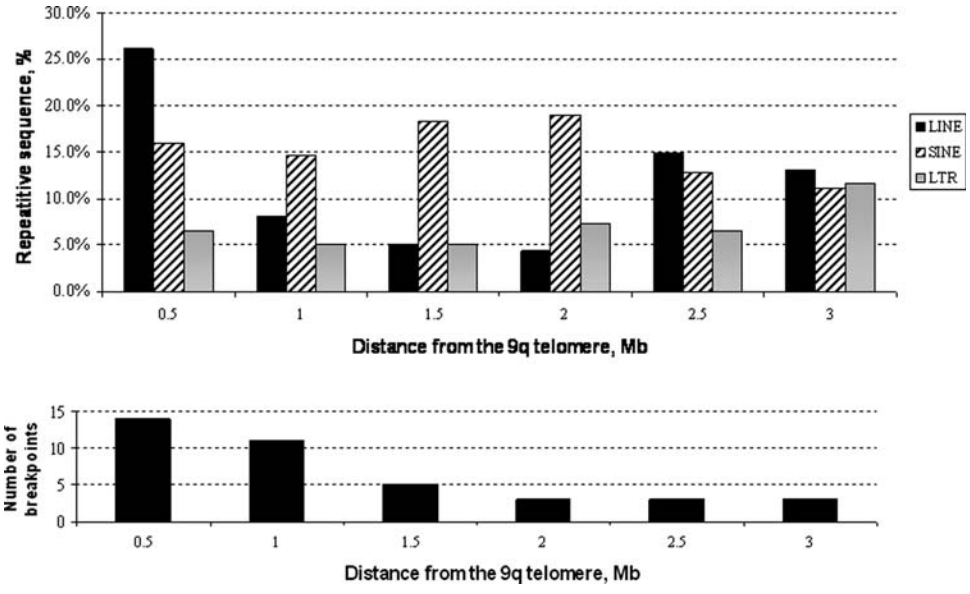

Figure 7. Density of repetitive elements and the breakpoints distribution within the most distal 9q34.3 region. (**A**) The histogram shows the content of various repetitive elements. (**B**) Distribution of the 9q34.3 breakpoints shows positive correlation from LINE repeats density.

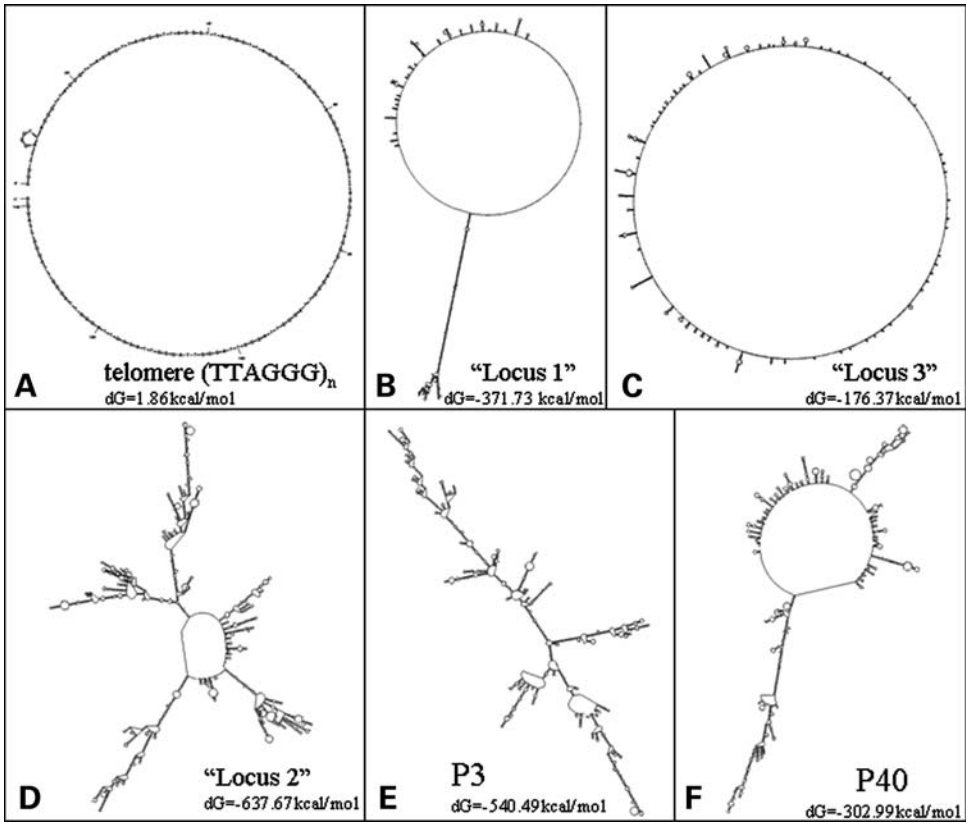

Figure 8. DNA secondary structures at the deletion breakpoints.

USA). A total of 26 655 probes were placed within a 10 Mb region of 9q34 (chr9: 129 961 525–140 153 008) with an average probe spacing of 375 bp. The most distal 120 kb region of 9q (chr9: 140 153 008–140 273 252), which contains TAR sequences, had no coverage on the custom 9q34 array. Approximately 4000 probes covering 1 Mb of every subtelomere region of all other chromosomes were interrogated with a density of one probe per 10 kb. The remaining 10 988

probes were positioned within coding and noncoding regions of selected genes to potentially allow the detection of genomic imbalances in other regions associated with a clinical presentation similar to 9q34.3 microdeletion syndrome. Nearly 2000 probes were used for quality control and normalization. Comprehensive probe coverage spans both coding and noncoding regions. Probes were carefully selected, optimized and validated for maximal sensitivity and specificity on several samples with known genomic aberrations. Such array-CGH design enables rapid detection of DNA copy number changes (i.e. genomic gains or losses) within the unique sequence of 9q34 subtelomere with a resolution of ~0.5–3 kb, as well as other subtelomeric regions. This resolution is sufficient to clone breakpoint junctions using conventional or long-range PCR (LR-PCR). Genomic DNAs were isolated from blood samples using the Puregene Kit (Gentra Systems, Minneapolis, MN, USA).

Gender-matched genomic DNAs obtained from either a normal male or female individual were used as reference DNA. The procedures for DNA digestion, labeling and hybridization were performed according to the manufacturer's instructions with some modifications. In brief, the patient and reference DNAs were digested with *Alu*I and *Rsa*I (Promega, Madison, WI, USA). Patient DNA was labeled with Cy5-dCTP and reference DNA with Cy3-dCTP by random priming using an array-CGH genomic labeling kit according to the manufacturer's instructions (Bioprime, Invitrogen Corp., Carlsbad, CA, USA). After labeling, DNAs were purified using the Microcon YM-30 column (Millipore, Billerica, MA, USA), incubated with human Cot-1 DNA (Invitrogen Corp.) and resuspended in hybridization buffer. The microarrays were hybridized using Agilent chambers for 40 h at 65°C, washed in wash buffer and rinsed with acetonitrile (Sigma-Aldrich Corp., St Louis, MO, USA) and with stabilization and drying solution. Slides were scanned using an Axon microarray scanner (GenePix 4000B from Axon Instruments, Union City, CA, USA). The acquired microarray images were quantified using Agilent feature extraction software 9.5.3, and then imported into Agilent CGH Analytics 3.4.4 software for analysis.

Whole Human Genome Oligonucleotide Microarray Kits (244K) (Agilent Technologies) were used to analyze DNA in two patients (P11 and P19), with additional chromosomal material at the distal long arm of 9q identified by cytogenetic studies.

Cytogenetic and FISH analyses

Metaphase chromosomes and interphase nuclei were obtained for all patients and their parents from PHA-stimulated blood lymphocyte cultures. Conventional G-banding and FISH analyses were performed as described with minor modifications (3). FISH experiments with BACs or fosmid clones labeled directly with Spectrum Orange-dUTP or Spectrum Green-dUTP using a commercially available kit (Abbot Molecular/Vysis) were employed for the confirmation of array-CGH results and for analysis of structural chromosome rearrangements. At least 10 metaphase and/or 50 interphase cells were scored for each hybridization. The telomere $(TTAGGG)_n$ repeats at the chromosome ends were detected by FISH analysis with All Human Telomeres Probe (Qbiogene/MP Biomedicals LLC, Tucson, AZ, USA) as specified by the manufacturer. Parental samples were screened to determine whether the 9q34.3 rearrangement represents a *de novo* or inherited event. The 9p (*305J–T7*) and 5q (*GS35o8/T7*, *D5S2907*) subtelomere-specific probes (Abbot Molecular/Vysis) were used to confirm unbalanced rearrangements in patient P11 and P38, respectively.

Amplification and sequencing of deletion junctions

For each patient, PCR primers were designed using genomic coordinates provided by interrogating oligonucleotides on our array that revealed the transition from loss/gain to normal DNA copy number. Breakpoint-surrounding DNA sequences were obtained from the UCSC Genome browser (http://genome.ucsc.edu, hg18 assembly). Several 'nested' primers were designed from both the proximal and the distal breakpoint segments, which were used in different combinations and orientations under various conditions until a unique product was amplified. Forward primers from the proximal 9q34.3 region and a reverse primer from the distal 9q34.3 region, or from a 5q35, or other 'donor' chromosome sequence, when the patient had a derivative chromosome, were used to amplify junction fragments in the patient with interstitial deletions or derivative chromosomes, respectively. In patients with terminal deletions, a breakpoint-specific primer and telomere primer TEL (5′-TCCCGAC-TATCCCTATCCC TATCCCTATCCCTATCCCTA-3′) were used as primer pairs for PCR. Patient-specific junctions were identified by comparison with parental controls.

Genomic DNA sequences were amplified using Qiagen HotStar*Taq* according to the manufacturer's protocol, with annealing temperatures ranging from 54 to 62°C. The reactions were performed in a total volume of 25 μl with 30 ng of template DNA, 1× buffer with variable concentrations of $MgCl_2$ and Q-solution, 200 μM of dNTPs, 100 nM of each primer and 0.625 U of HotStar*Taq* polymerase. LR-PCR reactions were carried out in 25 μl volume containing 2.5 U TaKaRa *LA Taq* (TaKaRa), 10× PCR buffer, a mixture of 2.5 mM of each dNTP, 50 ng of the patient's genomic DNA and 200 nM (final concentration) of each primer. An initial 5 min denaturation at 95°C was followed by 35 cycles of 1 min at 94°C, annealing at 55–60°C for 30 s, extension at 72°C for 1 min/kb and a final extension at 72°C for 7 min. Control samples from two normal male individuals and both parents (if available) were included in the PCR experiments. PCR products were visualized and their specificity was assessed by 1.2% TBE agarose gel electrophoresis. PCR products were excised from agarose gels and purified using a gel extraction kit (Qiagen). DNA sequencing was performed using either the ABI Prism BigDye v3.1 terminator kit or BigDye terminator chemistry (Applied Biosystems, Foster City, CA, USA) and an ABI 377 DNA sequencer or a 3730 DNA sequencer (Applied Biosystems). The chromatograms were analyzed using Sequencher 4.2 (Gene Codes).

Bioinformatics analysis of the deletion breakpoints

Different Web-based sequence-analysis programs were used to investigate the 2 kb genomic segments surrounding each

breakpoint in all patients (see WEB RESOURCES). BLAST was used for the analysis of sequence homologies, for repetitive elements and low-complexity sequences by the use of RepeatMasker (RepBase database version 7.4). The breakpoint sequences were compared against each other and themselves using the BLAST2 browser with default parameters. CLUSTALW was used to align the reference genomic sequence from both the proximal and distal breakpoint regions and abnormal recombinant junction sequence determined from each deletion or rearrangement event. The 300 bp regions surrounding the breakpoint were analyzed by Mreps and Palindrome software for palindromic sequences, the potential to form cruciforms, and tandem repeats. To predict secondary DNA structures, 40 pb and 3 kb sequences across each breakpoint were analyzed using Mfold version 3.1 (34) and compared with the recombinant junction sequences. Structures with the lowest free-energy values were selected for analysis.

Genotyping and parent-of-origin analysis

To investigate parent-of-origin for the rearrangements, we performed microsatellite and SNP analyses in the patient and in both parents (if available). Seven SNPs were used to study the parental origin of the deletions. To establish parent-of-origin, the deleted polymorphic loci alleles were compared between each patient and his (her) parents.

WEB RESOURCES

The accession number and URLs for data presented herein are as follows:

BLAST (BLASTn, BLASTz and BLAST2), http://www.ncbi.nlm.nih.gov/blast/
CLUSTALW, http://align.genome.jp/
Ensembl Genome Browser, http://www.ensembl.org/
Mfold, http://www.bioinfo.rpi.edu/applications/mfold/old/dna/
NCBI, http://www.ncbi.nih.gov/
Online Mendelian Inheritance in Man (OMIM), http://www.ncbi.nlm.nih.gov/Omim/
RepeatMasker, http://repeatmasker.org/
UCSC Genome Browser, http://genome.ucsc.edu/
The 9q34.3 community support group, http://www.9q34.org/

SUPPLEMENTARY MATERIAL

Supplementary Material is available at *HMG* online.

ACKNOWLEDGEMENTS

We thank the patients and their parents for participation in this research, and Marjorie Withers and Alexander Yatsenko for excellent technical assistance.

Conflict of Interest statement. None declared.

FUNDING

This study was supported in part by grants from the National Institute of Child Health and Human Development (PO1 HD39420) and the Mental Retardation Research Center (HD24064).

REFERENCES

1. Harada, N., Visser, R., Dawson, A., Fukamachi, M., Iwakoshi, M., Okamoto, N., Kishino, T., Niikawa, N. and Matsumoto, N. (2004) A 1-Mb critical region in six patients with 9q34.3 terminal deletion syndrome. *J. Hum. Genet.*, **49**, 440–444.
2. Iwakoshi, M., Okamoto, N., Harada, N., Nakamura, T., Yamamori, S., Fujita, H., Niikawa, N. and Matsumoto, N. (2004) 9q34.3 deletion syndrome in three unrelated children. *Am. J. Med. Genet.*, **126A**, 278–283.
3. Yatsenko, S.A., Cheung, S.W., Scott, D.A., Nowaczyk, M.J., Tarnopolsky, M., Naidu, S., Bibat, G., Patel, A., Leroy, J.G., Scaglia, F. *et al.* (2005) Deletion 9q34.3 syndrome: genotype–phenotype correlations and an extended deletion in a patient with features of Opitz C trigonocephaly. *J. Med. Genet.*, **42**, 328–335.
4. Kleefstra, T., Brunner, H.G., Amiel, J., Oudakker, A.R., Nillesen, W.M., Magee, A., Geneviève, D., Cormier-Daire, V., van Esch, H., Fryns, J.-P. *et al.* (2006) Loss-of-function mutations in euchromatin histone methyl transferase 1 (*EHMT1*) cause the 9q34 subtelomeric deletion syndrome. *Am. J. Hum. Genet.*, **79**, 370–377.
5. Simovich, M.J., Yatsenko, S.A., Kang, S.-H.L., Cheung, S.W., Dudek, M.E., Pursley, A., Ward, P.A., Patel, A. and Lupski, J.R. (2007) Prenatal diagnosis of a 9q34.3 microdeletion by array-CGH in a fetus with an apparently balanced translocation. *Prenat. Diag.*, **27**, 1112–1117.
6. Moyzis, R.K., Buckingham, J.M., Cram, L.S., Dani, M., Deaven, L.L., Jones, M.D., Meyne, J., Ratliff, R.L. and Wu, J.R. (1988) A highly conserved repetitive DNA sequence, $(TTAGGG)_n$, present at the telomeres of human chromosomes. *Proc. Natl Acad. Sci. USA*, **85**, 6622–6626.
7. Muller, H.J. (1938) The remaking of chromosomes. *Collecting Net*, **13**, 182–198.
8. McClintock, B. (1941) The stability of broken ends of chromosomes in Zea Mays. *Genetics*, **26**, 234–282.
9. Brown, W.R.A., Mackinnon, P.J., Villasante, A., Spurr, N., Buckle, V.J. and Dobson, M.J. (1990) Structure and polymorphism of human telomere-associated DNA. *Cell*, **63**, 119–132.
10. Flint, J., Bates, G.P., Clark, K., Dorman, A., Willingham, D., Roe, B.A., Micklem, G., Higgs, D.R. and Louis, E.J. (1997) Sequence comparison of human and yeast telomeres identifies structurally distinct subtelomeric domains. *Hum. Mol. Genet.*, **6**, 1305–1314.
11. Lee, J.A., Carvalho, C.M. and Lupski, J.R. (2007) DNA replication mechanism for generating nonrecurrent rearrangements associated with genomic disorders. *Cell*, **131**, 1235–1247.
12. Flint, J., Wilkie, A.O.M., Buckle, V.J., Winter, R.B., Holland, A.J. and McDermid, H.E. (1995) The detection of subtelomeric chromosomal rearrangements in idiopathic mental retardation. *Nat. Genet.*, **9**, 132–139.
13. Ledbetter, D.H. and Martin, C.L. (2007) Cryptic telomere imbalance: a 15-year update. *Am. J. Med. Genet.*, **145C**, 327–334.
14. Shao, L., Shaw, C.A., Lu, X.Y., Sahoo, T., Bacino, C.A., Lalani, S.R., Stankiewicz, P., Yatsenko, S.A., Li, Y., Neill, S. *et al.* (2008) Identification of chromosome abnormalities in subtelomeric regions by microarray analysis: a study of 5,380 cases. *Am. J. Med. Genet.*, **146A**, 2242–2251.
15. Lupski, J.R. (1998) Genomic disorders: structural features of the genome can lead to DNA rearrangements and human disease traits. *Trends Genet.*, **14**, 415–420.
16. Heilstedt, H.A., Ballif, B.C., Howard, L.A., Lewis, R.A., Stal, S., Kashork, C.D., Bacino, C.A., Shapira, S.K. and Shaffer, L.G. (2003) Physical map of 1p36, placement of breakpoints in monosomy 1p36, and clinical characterization of the syndrome. *Am. J. Hum. Genet.*, **72**, 1200–1212.
17. Christ, L.A., Crowe, C.A., Micale, M.A., Conroy, J.M. and Schwartz, S. (1999) Chromosome breakage hotspots and delineation of the critical region for the 9p-deletion syndrome. *Am. J. Hum. Genet.*, **65**, 1387–1395.

18. Kong, A., Gudbjartsson, D.F., Sainz, J., Jonsdottir, G.M., Gudjonsson, S.A., Richardsson, B., Sigurdardottir, S., Barnard, J., Hallbeck, B., Masson, G. *et al.* (2002) A high-resolution recombination map of the human genome. *Nat. Genet.*, **31**, 241–247.
19. Matise, T.C., Chen, F., Chen, W., De La Vega, F.M., Hansen, M., He, C., Hyland, F.C., Kennedy, G.C., Kong, X., Murray, S.S. *et al.* (2007) A second-generation combined linkage physical map of the human genome. *Genome Res.*, **17**, 1783–1786.
20. Stankiewicz, P. and Lupski, J.R. (2002) Genome architecture, rearrangements and genomic disorders. *Trends Genet.*, **18**, 74–82.
21. Gu, W., Zhang, F. and Lupski, J.R. (2008) Mechanisms for human genomic rearrangements. *Pathogenetics*, **1**, 4.
22. Flint, J., Rochette, J., Craddock, C.F., Dode, C., Vignes, B., Horsley, S.W., Kearney, L., Buckle, V.J., Ayyub, H. and Higgs, D.R. (1996) Chromosomal stabilization by a subtelomeric rearrangement involving two closely related *Alu* elements. *Hum. Mol. Genet.*, **5**, 1163–1169.
23. Ballif, B.C., Gajecka, M. and Shaffer, L.G. (2004) Monosomy 1p36 breakpoints indicate repetitive DNA sequence elements may be involved in generating and/or stabilizing some terminal deletions. *Chromosome Res.*, **12**, 133–141.
24. Bacolla, A. and Wells, R.D. (2004) Non-B DNA conformations, genomic rearrangements, and human disease. *J. Biol. Chem.*, **279**, 47411–47414.
25. Slack, A., Thornton, P.C., Magner, D.B., Rosenberg, S.M. and Hastings, P.J. (2006) On the mechanism of gene amplification induced under stress in *Escherichia coli*. *PLoS Genet.*, **2**, e48.
26. Hastings, P.J. (2007) Adaptive amplification. *Crit. Rev. Biochem. Mol. Biol.*, **42**, 271–283.
27. Hastings, P.J., Ira, G. and Lupski, J.R. (2009) A microhomology-mediated break-induced replication model for the origin of human copy number variation. *PLoS Genet.*, **5**, e1000327.
28. Gijsbers, A.C., Bijlsma, E.K., Weiss, M.M., Bakker, E., Breuning, M.H., Hoffer, M.J. and Ruivenkamp, C.A. (2008) A 400 kb duplication, 2.4 Mb triplication and 130 kb duplication of 9q34.3 in a patient with severe mental retardation. *Eur. J. Med. Genet.*, **51**, 479–487.
29. Flint, J., Craddock, C.F., Villegas, A., Bentley, D.P., Williams, H.J., Galanello, R., Cao, A., Wood, W.G., Ayyub, H. and Higgs, D.R. (1994) Healing of broken human chromosomes by the addition of telomeric repeats. *Am. J. Hum. Genet.*, **55**, 505–512.
30. Ballif, B.C., Kashork, C.D. and Shaffer, L.G. (2000) FISHing for mechanisms of cytogenetically defined terminal deletions using chromosome-specific subtelomeric probes. *Eur. J. Hum. Genet.*, **8**, 764–770.
31. Varley, H., Di, S., Scherer, S.W. and Royle, N.J. (2000) Characterization of terminal deletions at 7q32 and 22q13.3 healed by *de novo* telomere addition. *Am. J. Hum. Genet.*, **67**, 610–622.
32. Wong, A.C.C., Ning, Y., Flint, J., Clark, K., Dumanski, J.P., Ledbetter, D.H. and McDermid, H.E. (1997) Molecular characterization of a 130-kb terminal microdeletion at 22q in a child with mild mental retardation. *Am. J. Hum. Genet.*, **60**, 113–120.
33. Bonaglia, M.C., Giorda, R., Mani, E., Aceti, G., Anderlid, B.M., Baroncini, A., Pramparo, T. and Zuffardi, O. (2006) Identification of a recurrent breakpoint within the *SHANK3* gene in the 22q13.3 deletion syndrome. *J. Med. Genet.*, **43**, 822–828.
34. Zuker, M. (2003) Mfold web server for nucleic acid folding and hybridization prediction. *Nucleic Acids Res.*, **31**, 3406–3415.